TURBULENT OPEN-CHANNEL FLOW OVER A PERMEABLE BED

Thorsten Stoesser[(1)], Jochen Fröhlich[(2)], Wolfgang Rodi[(3)]

[(1)]School of Civil and Environmental Engineering, Georgia Institute of Technology, 790 Atlantic Drive, Atlanta, GA, 30332, USA
phone: +1 404 894 4432; fax: +1 404 894 2278; e-mail: thorsten@ce.gatech.edu
[(2)]Institute for Technical Chemistry and Polymer Chemistry, University of Karlsruhe, 76128 Karlsruhe, Germany
phone: +49 721 6083206; fax: +49 721 6084820; e-mail: froehlich@ict.uni-karlsruhe.de
[(3)]Institute for Hydromechanics, University of Karlsruhe, 76128 Karlsruhe, Germany
phone: +49 721 6083535; fax: +49 721 6087712; e-mail: rodi@ifh.uka.de

ABSTRACT

This paper presents results of a Large Eddy Simulation (LES) of turbulent flow in an open channel over and through 3 layers of spheres, which can be regarded as an idealized permeable bed. The setup and boundary conditions are selected analogous to recently completed laboratory experiments. The mean streamwise velocities from the LES are compared to the measured data in order to validate the calculations. Due to a high porosity of the bed there is considerable momentum exchange between the flow above and within the spheres, which produces additional shear stresses and hence leads to velocity and turbulence intensity distributions differing considerably from those over solid beds. The overall agreement between calculated and measured mean streamwise velocities above the bed is very satisfying. Below the roughness interface flow velocities, turbulence intensities and pressure fluctuations are damped exponentially. The damping of pressure fluctuations has also been observed from pressure measurements in a porous gravel bed. Furthermore, coherent flow structures (like sweeps and ejections) are suggested to be the driving mechanism of momentum exchange between the two flow regions.

Keywords: turbulence, open-channel flow, large-eddy simulation, rough wall, permeable wall

1 INTRODUCTION

Although almost all natural channels have permeable beds such as gravel-bed rivers, very little research has been undertaken in order to study the effect of channel bed permeability on the mean and instantaneous flow. In common practice a permeable bed has usually been treated analogously to an impermeable bed and flow resistance coefficients and velocity distributions were derived irrespective of bed porosity. However, depending on the permeability of the subsurface, significant interaction processes occur between the flow above the porous bed and the subsurface area. The effects of interaction are a non-zero velocity at the permeable boundary and the existence of turbulent exchange of mass and momentum between the two flow regions. These exchange processes are responsible for additional shear stresses near the boundary (Nezu, 1977). Lovera and Kennedy (1969), Zagni and Smith (1976), and Zippe and Graf (1983), for instance, have shown that the overall friction loss in a flow over a permeable bed is larger than over an equivalent impermeable bed. The driving force which is responsible for the exchange processes between the pore layer and the upper flow is the presence of local pressure gradients, a mechanism similar to the interaction between the turbulent boundary layer and the viscous sublayer in the flow over a smooth bed. These local pressure gradients are generated by the dynamics of the turbulent flow over (smooth, rough, and permeable) boundaries, where the flow field is dominated by energetic three-dimensional organized (coherent) vortical structures. Over 4 decades of experimental work have been dedicated to the identification of the physical processes which govern these coherent structures, and much progress has been made in recent years due to the advances in measurement techniques and in numerical simulation methods associated with the growth in

speed and capacity of modern supercomputers. While the flow physics of coherent structures over smooth surfaces is understood fairly well (see the summary by Robinson, 1991), the flow over rough impermeable and permeable walls is still an area of active turbulence research. The reason is the existence of a wide variety of possible wall roughness geometries as well as permeability conditions and recent research endeavours have shown that the details of the geometry influence the flow across the entire turbulent layer (Jiménez, 2004). As a consequence, the distribution of mean flow velocities and higher order turbulent statistics differ considerably from those over smooth walls in a region usually called the "roughness sublayer", which is a layer adjacent to the rough (im)permeable bed. There have been numerous research efforts recently to quantify the effects of (impermeable) roughness on the mean flow statistics (see the most recent summary by Jiménez, 2004) or to elucidate the turbulent instantaneous flow structures (Stoesser et al., 2004) over impermeable rough beds. Studies of turbulent flow over permeable beds are very scarce. There has been few experimental work on quantification of the friction loss (Zagni and Smith, 1976, Zippe and Graf, 1983), on the determination of the vertical velocity profile for the flow above the permeable bed (Kong and Schetz, 1982, Gupta and Paudyal, 1986, Zagni and Smith, 1976, Zippe and Graf 1983, Nakagawa et al., 1991, Dancey et al., 2000), as well as on the collection of pressure and velocity signals within the permeable bed (Detert et al., 2004). There are several numerical studies of flow over and/or through porous media which use an integral numerical approach like the Volume Average Navier Stokes approach (Breugem and Boersma, 2005) or apply adequate slip-conditions (Jiminez et al., 2001), but these methods do not resolve the details of the interaction between the two layers, hence important physical mechanisms may be neglected. Directly resolving the details of the flow geometry of a porous media is extremely complex and tremendously expensive, especially for natural permeable beds. To our knowledge only one study represents the porous media directly: Breugem and Boersma (2005) performed a DNS over and through a permeable bed that consisted of an array of cubes, with the main objective of validating a previously developed integral approach.

In this paper we present the results of an LES of open-channel flow over a permeable wall that consists of three layers of spheres. This is the first detailed numerical study of the flow over a permeable bed that has also been investigated in a laboratory experiment. The main purpose of this study is to provide further insight into the turbulent flow over permeable beds and to enhance the understanding of the effect of bed permeability on the mean and instantaneous flow. Temporal and spatial averaging is used to quantify the effects on the flow velocities and the turbulent fluctuations.

2 NUMERICAL FRAMEWORK

The LES code MGLET, originally developed at the Institute for Fluid Mechanics at the Technical University of Munich (Tremblay and Friedrich, 2001), was used to perform the Large Eddy Simulations. The code solves the filtered Navier-Stokes equations discretised with a finite-volume method on a staggered Cartesian grid. Convective and diffusive fluxes are approximated with central differences of second order accuracy and time advancement is achieved by a second order, explicit Adams-Bashford scheme. A Poisson equation is solved to couple the pressure to the velocity field. The subgrid-scale stresses appearing in the filtered Navier-Stokes equations are computed using the dynamic approach of Germano *et al.* (1991). The no-slip boundary condition is applied on the surface of the spheres where the immersed boundary method is employed (Verzicco *et al.*, 2000). This method is a combination of applying body forces in order to block the cells that are fully inside the sphere and a Lagrangian interpolation scheme of third order, which is used for the cells that are intersected by the spheres' surface to maintain the no-slip condition (Tremblay and Friedrich, 2001).

3 SETUP AND BOUNDARY CONDITIONS

The setup and boundary conditions of the Large Eddy Simulation were selected in analogy to flume experiments performed at the University of Aberdeen by Prokrajac (2005), where spheres of $d=12mm$ diameter were placed in three layers on the flat flume bottom. The flow depth from the roughness tops to the free surface is $H=41\ mm$ which gives a relative submergence ratio of $H/D=3.42$. The depth averaged bulk velocity is $U=0.37\ m/s$, which yields a Reynolds number of $Re= UH/n \approx 15200$. Mean and turbulent flow velocities were measured with a 2D Particle Image Velocimetry (PIV) system along two longitudinal (x-z) planes above the spheres. These measurements were used in order to validate the results of the LES computations. The computational domain of the surface flow region spans $5.3H$ x $3.5H$ x H. The subsurface region consisted of 3 layers of spheres of diameter D arranged in a cubical pattern with 18 x 12 spheres per layer (see Figure 1). A very high resolution grid consisting of $720 \times 480 \times 216$ points for the computation domain was employed, which is approximately 75 million grid points in total. Hence, each sphere is resolved with 40 points over the diameter. Based on the global wall shear stress, the grid spacings in terms of wall units are $?x^+ \sim 8$ in streamwise direction and $?y^+ \sim 8$ in spanwise direction. In the vertical direction the grid spacing was kept at a constant value of $?z^+ \sim 1.0$ from the bed to the top of the spheres and was stretched above the spheres towards the surface. A part of the grid, where only every 5^{th} grid line is plotted, and the details of the grid around one sphere are shown in Figure 2. It has to be noted that due to the third order interpolation scheme of the immersed boundary method the touching point is not a singular point but an area consisting of 3 x 3 grid points. This is the reason why later on in plots with maximum porosity a trace of the sphere is still visible. Periodic boundary conditions were applied in the streamwise and spanwise directions.

4 RESULTS AND DISCUSSIONS

4.1 Mean Flow Field

Figure 3 shows contours of the time-averaged flow along a longitudinal plane with minimum porosity (as indicated with the sketch near the top of the image) for both LES (left) and the experiment. Overall the match between simulation and experiment is very good and differences can only be observed near the spheres, where the LES predicts a more pronounced waviness of the flow, which is caused by the flow accelerating above the roughness tops. Between the roughness elements near the sphere tops there is a small recirculation region, caused by separation at the top of the spheres. This small-scale behaviour could not be measured in the laboratory due to the resolution of the camera. Figure 4 compares mean flow velocities between LES and experiments in a longitudinal plane with maximum porosity i.e. where the spheres touching each other (see sketch). Again the agreement between measured and calculated flow velocities is very good. Due to the relatively large porosity of the setup there is considerable flow in the pore region, which could not be measured in the experiment.

Figure 5 shows a more quantitative comparison of mean streamwise flow velocities along vertical lines through the centre between two spheres ($x/D=0.5$, *red line*) and through the centre of one sphere ($x/D=1$, *blue line*) in longitudinal planes with minimum porosity (left) and maximum porosity (right). As was shown before, the prediction of the mean streamwise velocity is in fairly good agreement with the observed data and there are only small differences. The streamwise velocity profiles collapse relatively early at about $0.2D$ above the top of the sphere, which suggests the existence of only a thin roughness layer, i.e. the layer where the flow "feels" the details of the roughness geometry. However, recirculation behind the spheres and a certain amount of flow through the pores can be seen clearly. It is evident that the flow velocities in the first pore are noticeably smaller than in the second pore and near the flume bed. This has also been reported by Prokrajac (2005) and is now confirmed with the

present LES. The reason for this behaviour is that the turbulent exchange process between the outer flow region and pore region causes a retardation of the streamwise flow in the first layer or in the first pores respectively. The protrusion of turbulence into the pores can be visualized with streamwise and wall normal turbulence intensities. Figure 6 shows the streamwise (left) and wall-normal (right) velocity fluctuations in a longitudinal slice with maximum porosity. The highest values are observed in the "roughness layer" i.e. the area just above the permeable bed where the highest shear is known to occur. It can be seen that considerable turbulence intrudes into the subsurface area and the effect of mass and momentum exchange becomes obvious from the fairly high values of wall-normal fluctuations in the interface region. Further below, i.e. in the second and third layer of spheres, there is still some turbulence left, however the amount is considerably lower.

Figure 7(left) shows a similar picture for the pressure fluctuations in a plane with maximum porosity. The peaks of the fluctuations appear at the windward side near the top of the spheres. Comparison with Figure 6 shows that they are partly due to *u*-fluctuations and close to the sphere related to other Reynolds stresses. The pressure fluctuations also intrude into the pores, and this is strongest near the top of the layer. In planes with minimum porosity, fluctuations with a similar magnitude are seen in the interstitial. The magnitude of pressure fluctuations is quantified by Figure 8, where these are given along a spatially averaged line. It is interesting to see that this curve has a pronounced peak slightly below the top of the spheres. This is in line with the inclined red spots visible in Figure 7 at these locations. For comparison, experimental data of (Detert et al., 2004) have been included in this figure as well. These authors measured pressure signals along a vertical in the flow above and through a naturally packed gravel bed. The form of the decay of fluctuations with the depth is very similar and follows an exponential curve. However, the level of pressure fluctuations in the experiment is somewhat lower, due to the much denser packing of natural gravel in comparison to our artificial sphere arrangement. The large experimental value at $z=D$ can be explained by the high regularity of the present arrangement compared to natural gravels and the fact that this is a point measurement at a single location (probably exactly above a gravel). Values of pressure fluctuations that are up to 6 times larger than the mean wall shear stress were also observed in our calculations (see Figure 7).

4.2 Instantaneous Flow Field

Figure 9 shows a snapshot of the perturbation vector field (*u'-w'*) in two selected *x-z* planes with maximum (left) and minimum (right) porosity respectively. It is apparent from the magnitude of the perturbation vectors that most of the turbulence occurs in the roughness sublayer just above the spheres. In the slice with maximum porosity in- and outflow scenarios are visible. Furthermore, sweep (i.e. u'>0 and w'<0) and ejection (i.e. u'<0 and w'>0) events can be seen near the permeable bed, comparable to those observed over smooth beds (as described in Robinson, 1991) and rough beds (Stoesser et al. 2003). The instantaneous data are currently being analyzed using a quadrant analysis, similarly to the one in Stoesser et al. (2003).

Finally, time signals at individual points are considered in Figure 10. The positions where timesignals were extracted are just above the top of the spheres and in the centre of the two pores as indicated in Figure 7 (left). The raw time signals not only show large fluctuations of the velocity components but also high intermittency in the pores. In particular, for the first pore the *w*-velocity peaks are spaced by very large time intervals. These peaks may be attributed to sweep events occurring at specific instants in time. This is supported by the fact that during these sweep events the peaks in *w* attain higher values than those in *u*, because the fluid with large u' and large (negative) w' enters the permeable layer and the momentum is directed to the lower area of the porous bed. Above the spheres in the bulk flow, the *u*-

fluctuations dominate and exhibit strong intermittency due to the coherent structures mentioned above. The spectra in the right column of this figure were obtained from the time signals displayed. For better understanding they are arranged such that the same quantity at different elevations is displayed in one graph. In the outer flow the streamwise velocity spectra exhibit a -5/3-range until a frequency of about 1. Beyond, there is a slower decay of the spectrum, until a frequency of about 5, and further than that the strong decay induced by the LES approach appears. Within the pores, the distribution of the energy is almost parallel to the bulk flow spectra but with less energy. The damping of the large-scale streamwise fluctuations is substantially stronger than for the wall-normal fluctuations in the first pore and the spectra become more isotropic. In the second pore there is about a decade difference in energy with respect to the outer signal. Also, the frequency where the somewhat stronger decay starts is lowered from the first to the second pore. The pressure fluctuations exhibit similar behaviour. The exponential damping of the pressure is also expressed in the spectra and the slope in the pore region steepens already at frequencies of 1. Very interesting is the pronounced peak in the pressure spectrum at a frequency of 0.06. In the pores it is even stronger than at the considered point in the outer flow. This effect is related to the peak in the *u*-spectrum at the same frequency. Hence, a trace of the large coherent structures in the outer flow is clearly seen even in the second pore.

5 CONCLUSIONS

The paper has presented the results of a Large Eddy Simulation of open channel flow over a permeable bed that consisted of 3-layers of spheres. These are capable of resolving the unsteady flow around and between the individual spheres to a very high degree and provide an enormous wealth of data. The calculated mean velocities showed generally good agreement with the measured data of Prokrajac (2005). First findings concerning higher order statistics, flow structures and spectral content of the flow were reported. These are currently extended in ongoing work.

AKNOWLEDGMENTS

This work is part of a research project funded by the German Research Foundation (DFG) under project number Ji 18/10-3. The computations were carried out on the IBM SP-SMP of the scientific supercomputing centre (SSCK) at the University of Karlsruhe. The provision of the experimental data by Dr. Dubravka Prokrajac and the successful collaboration with the Department of Engineering at the University of Aberdeen is acknowledged gratefully.

REFERENCES

Breugem, W.P., Boersma, B.J. (2005) Direct Numerical Simulations of Turbulent Flow Over a Permeable Wall Using A Direct And A Continuum Approach. *Physics of Fluids*, 17(2).

Dancey, C.L., Balakrishnan, M., Diplas, P., Papanicolaou, A.N. (2000) The Spatial Inhomogeneity of Turbulence Above a Fully Rough, Packed Bed in Open Channel Flow", *Experiments in Fluids*, 29, pp. 402-410.

Detert, M., Jirka, G.H., Jehle, M., Klar, M,. Jähne, B., Köhler, H.-J., Wenka, T. (2004) Pressure Fluctuations Within Subsurface Gravel Bed Caused by Turbulent Open-Channel Flow, *Proc. River Flow 2004*, M. Greco (Ed.), Napoli, Italy

Germano M., Piomelli U., Moin P., Cabot W. H. (1991). A Dynamic Subgrid-scale Eddy Viscosity Model. *Physics of Fluids*, 3(7), 1760-1765.

Gupta, A. D., Paudyal, G. N. (1985) Characteristics of Free Surface Flow over a Gravel Bed. Journal of Irrigation and Drainage Engineering. Vol. 111, no. 4, pp. 299-318.

Jimenez, J. (2004). Turbulent Flows Over Rough Walls. *Annu. Rev. Fluid Mech.*, 36, 173–96.

Jiménez, J., Uhlmann, M., Pinelli, A., Kawahara, G. (2001). Turbulent Shear Flow over

Active and Passive Porous Surfaces. *J. of Fluid Mechanics*, Vol. 442 No. 9, pp 89-117.
Kong, F. Y., Schetz, J. A. (1982) Turbulent Boundary Layer over Porous Surfaces with Different Geometries. *AIAA Paper* 82-0030.
Lovera, F., Kennedy, J. F. (1969). Friction-Factors for Flat-Bed Flows in Sand Channels *ASCE J Hydraul Div*, Vol. 95, No 4, pp 1227-1234.
Nakagawa, H., Tsujimoto, T., Shimizu, Y. (1991). Turbulent Flow with Small Relative Submergence. *Fluvial Hydraulics of Mountain Regions*. Editor: A. Armanini, G. Di Silvio, Lecture Notes in Earth Sciences, Vol. 37, pp.33-44
Nezu, I. (1977). "Turbulent Structure in Open-Channel Flows." Ph.D Thesis, Dept. of Civil Engineering, Kyoto Univ., Japan.
Prokrajac (2005). Personal Communication
Robinson, K. (1991). Coherent Motions in the Turbulent Boundary Layer, *Ann. Rev. Fluid Mech*. Vol. 23. pp 601-639.
Stoesser, T., Fröhlich, J., Rodi W. (2003). Identification of Coherent Flow Structures in Open Channel Flow over Rough Bed Using Large Eddy Simulation. *Proceedings XXX IAHR Congress*, Thessaloniki, Greece.
Stoesser, T., Rodi, W., Fröhlich, J. (2005). Large Eddy Simulation of Open-Channel Flow Over a Layer of Spheres. In: *Proc. of 31st IAHR Congress*, Seoul, Sep. 11-16.
Stone, H.L. (1968). Iterative Solution of Implicit Approximation of Multi-dimensional Partial Differential Equations. *SIAM J. Numerical Analysis*. No. 3.
Tremblay, F., Friedrich, R. (2001). An Algorithm to Treat Flows Bounded by Arbitrarily Shaped Surfaces with Cartesian Meshes. In: *Notes on Numerical Fluid Mechanics*, Vol. 77, Springer.
Verzicco, R., Mohd-Yusof, J., Orlandi, P., Haworth, D. (2000). Large Eddy Simulation in Complex Geometric Configurations Using Boundary Body Forces. *AIAA J.* 38 (3). pp 427ff.
Zagni, A. F. E., Smith, K. V. H. (1976). Channel Flow over Permeable Beds of Graded Spheres. *ASCE, J. of the Hydraulics Division*, Vol. 102, No. 2. pp 207-222.
Zippe, H. J, Graf, W. H. (1983). Turbulent Boundary-Layer Flow over Permeable And Non-Permeable Rough Surfaces. *J. of Hydraulic Research* Vol. 21, No. 1, pp 51-65.

FIGURES

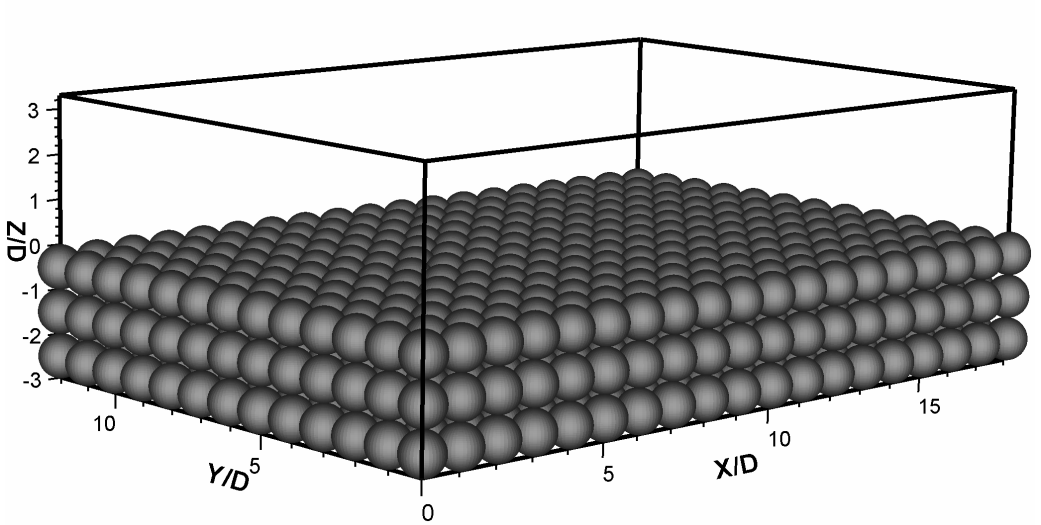

Figure 1: Computational domain and arrangement of spheres for the simulation performed.

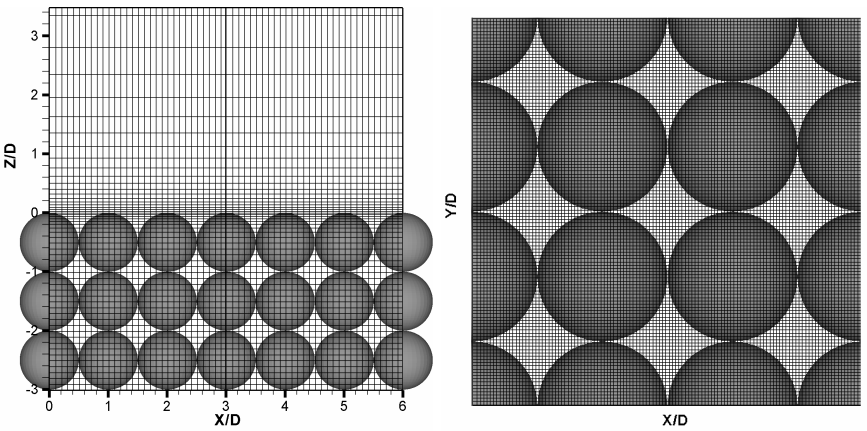

Figure 2: Details of the grid in a vertical plane (left) and a horizontal plane going through the centres of the spheres (right). In the left plot every 5th grid line is shown, in the right plot each gridline is displayed.

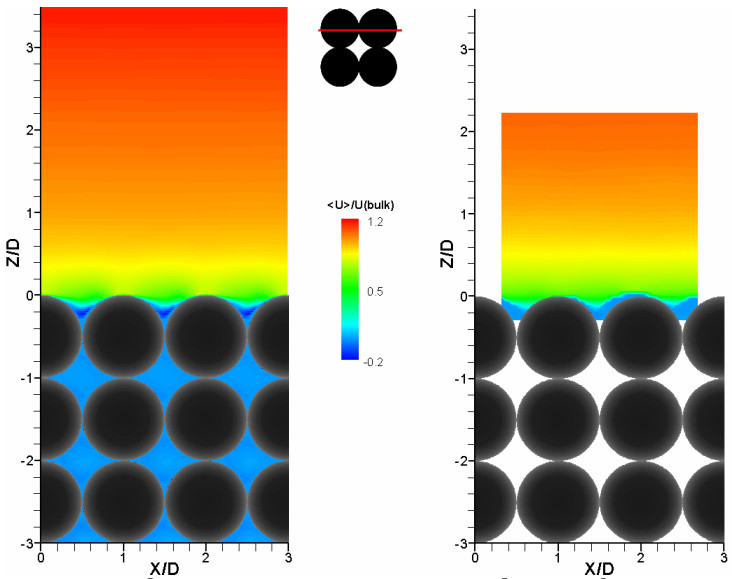

Figure 3: Mean streamwise velocity component in an *x-z* plane with minimum porosity (LES left, Experiment by Pokrajac (2005), right). The small sketch in the upper part indicates the position of the plane in a top view.

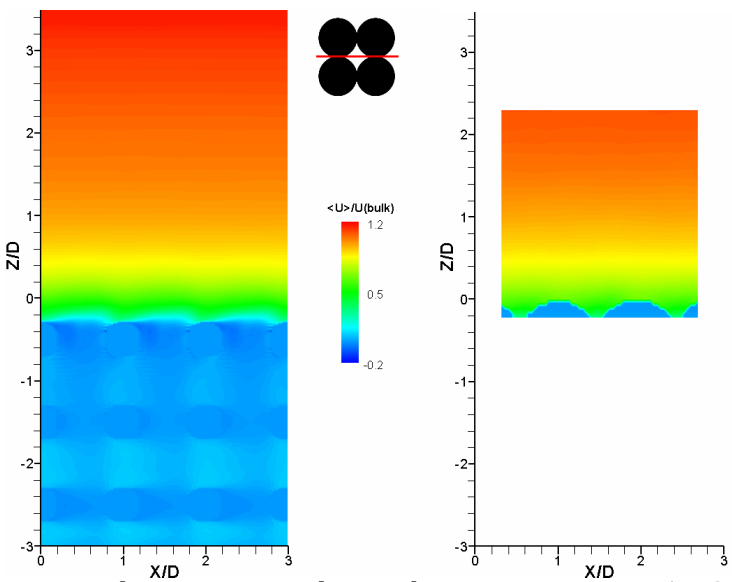

Figure 4: Mean streamwise velocity in an x-z plane with maximum porosity (LES left, Exp. right).

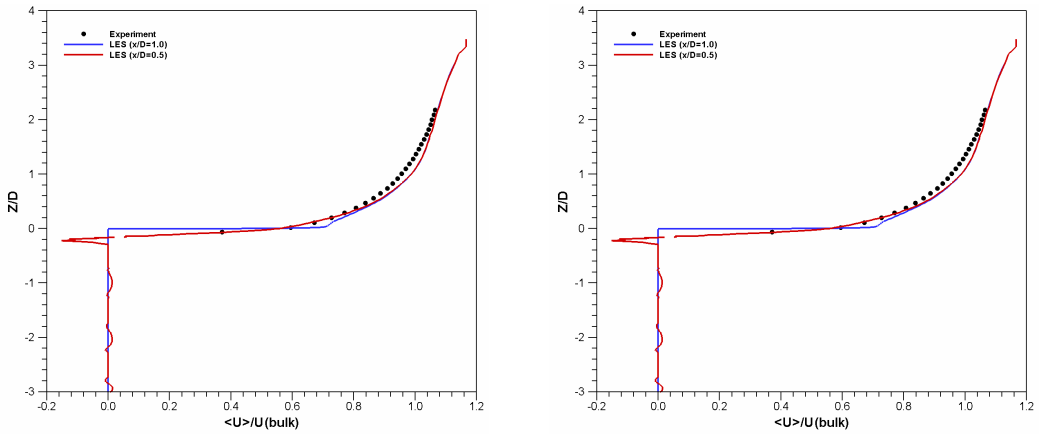

Figure 5: Vertical distribution of mean streamwise velocity along *x/D*=0.5 (red line) and *x/D*=1.0 (blue line) in planes with minimum (left) and maximum porosity (right).

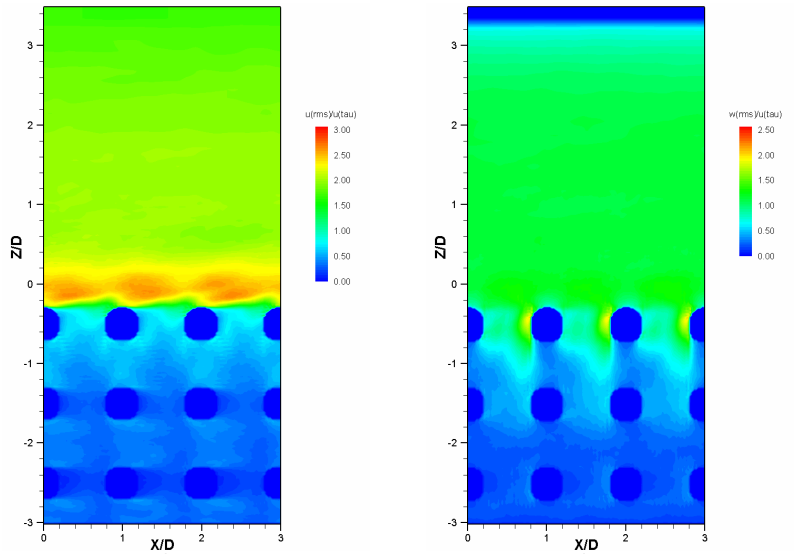

Figure 6: Predicted streamwise (left) and wall-normal (right) velocity fluctuations in an *x*-*z* plane with maximum porosity.

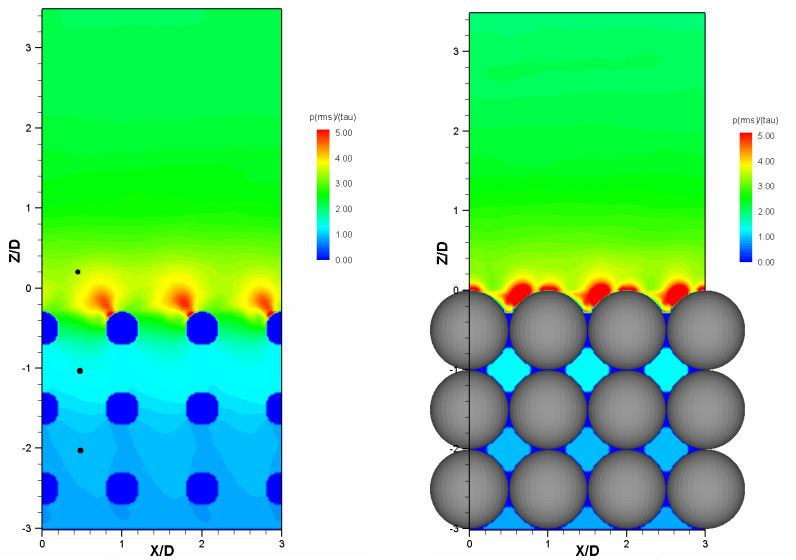

Figure 7: Predicted pressure fluctuations in an *x*-*z* plane with minimum (left) and maximum porosity (right). The black circles in the figure on the left hand side indicate locations where timesignals were extracted.

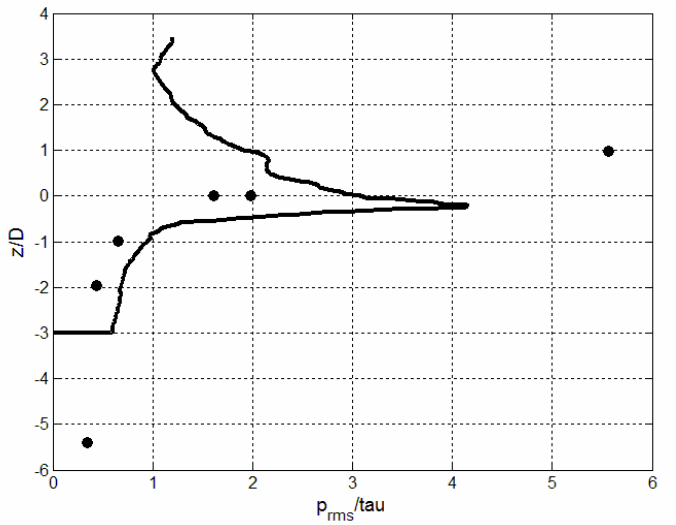

Figure 8: Spatially averaged vertical distribution of pressure fluctuations; Continuous line: LES, symbols: Experiment of Detert *et al.* 2004.

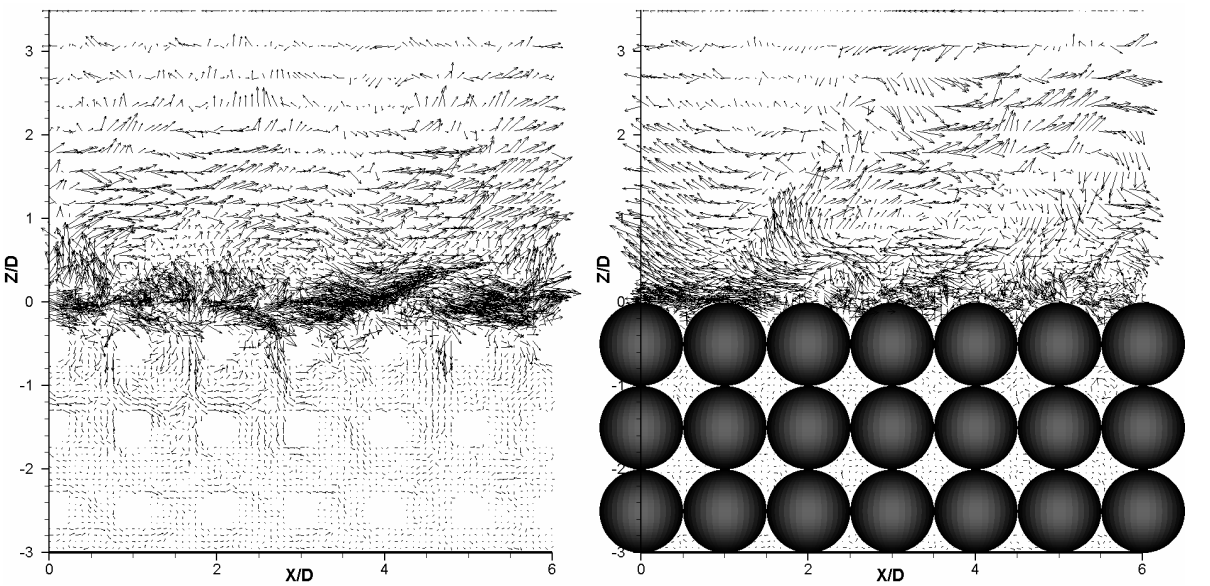

Figure 9: Perturbation vectors (*u'-w'*) in *x-z* planes with maximum (left) and minimum (right) porosity from LES.

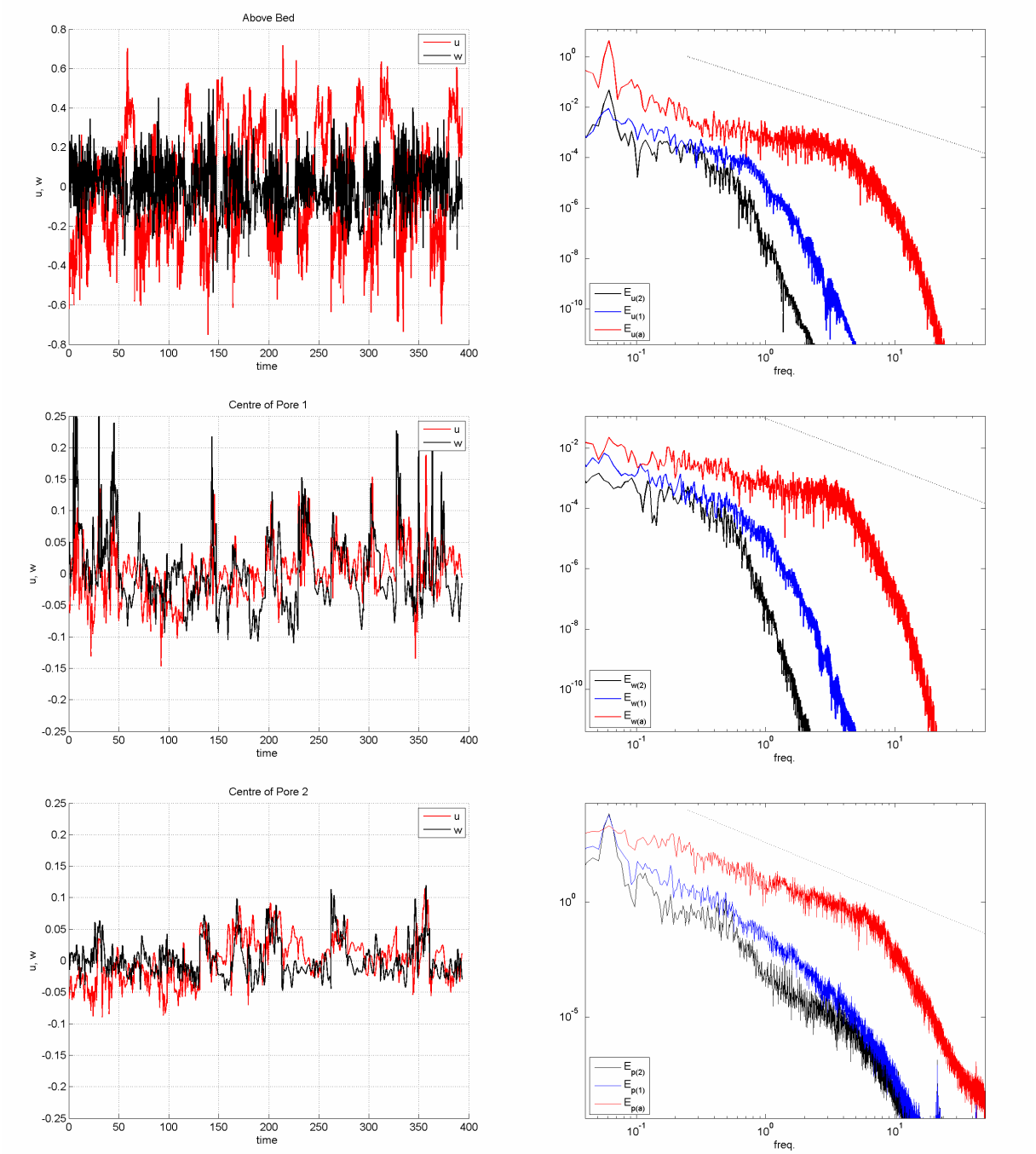

Figure 10: Time series and their analysis. (Locations are indicated in Figure 7 left). *Left:* Time signal of streamwise (red) and wall-normal (black) velocity fluctuations sampled over 390 time units. Top: position *(x, y, z)* = (*0.5D, 0.5D, 0.1D*), i.e. above the top of the spheres. Middle: position *(x, y, z) = (0.5D, 0.5D, -1D)*, i.e. in the centre of the first pore between the first and the second layer from above. Bottom: position *(x, y, z) = (0.5D, 0.5D, -2DD)*, in the centre of the second pore between the second and the third layer from above. *Right:* Power spectrum density of *u*, *w* and *p* at the corresponding points. Top: *u*-velocity Middle *w*-velocity, Bottom: pressure. First (red), second (blue) and third signal (black) are the outer, pore 1 and pore 2 signals, respectively. The straight line in the velocity spectra has a slope of -5/3 and a slope of -7/3 in the pressure spectra.